Journal of Biomechanics 128 (2021) 110773

Contents lists available at ScienceDirect

Journal of Biomechanics

journal homepage: www.elsevier.com/locate/jbiomech

Local and global growth and remodeling in calcific aortic valve disease and aging

Mohammadreza Soltany Sadrabadi [a], Mona Eskandari [b,c,d], Heidi P. Feigenbaum [a], Amirhossein Arzani [a,*]

[a] Department of Mechanical Engineering, Northern Arizona University, Flagstaff, AZ, USA
[b] Department of Mechanical Engineering, University of California Riverside, Riverside, CA, USA
[c] BREATHE Center at the School of Medicine, University of California Riverside, Riverside, CA, USA
[d] Department of Bioengineering, University of California Riverside, Riverside, CA, USA

ARTICLE INFO

Keywords:
Calcification
Mechanobiology
Kinematic growth
Multiscale modeling
Aortic stenosis

ABSTRACT

Aging and calcific aortic valve disease (CAVD) are the main factors leading to aortic stenosis. Both processes are accompanied by growth and remodeling pathways that play a crucial role in aortic valve pathophysiology. Herein, a computational growth and remodeling (G&R) framework was developed to investigate the effects of aging and calcification on aortic valve dynamics. Particularly, an algorithm was developed to couple the global growth and stiffening of the aortic valve due to aging and the local growth and stiffening due to calcification with the aortic valve transient dynamics. The aortic valve dynamics during baseline were validated with available data in the literature. Subsequently, the changes in aortic valve dynamic patterns during aging and CAVD progression were studied. The results revealed the patterns in geometric orifice area reduction and an increase in the valve stress during local and global growth and remodeling of the aortic valve. The proposed algorithm provides a framework to couple mechanobiology models of disease growth with tissue-scale transient structural mechanics models to study the biomechanical changes during cardiovascular disease growth and aging.

1. Introduction

Aortic stenosis is the most common form of valvular disease (Carabello and Paulus, 2009) and its prevalence is expected to increase due to an aging population (Thaden et al., 2014). Calcific aortic valve disease (CAVD) is a common cause of aortic stenosis, which is accompanied by thickened and stiffened calcified leaflets that compromise valve's normal opening and closure (Otto et al., 1997; Pawade et al., 2015). The process of calcification is a multistage and multiscale process (Weinberg et al., 2010; Pawade et al., 2015; Arzani et al., 2017) where a combination of biochemical and mechanical processes regulate calcification growth. Calcification influences aortic valve dynamics and blood flow physics around the leaflets (Hatoum et al., 2018; Hatoum and Dasi, 2019). Additionally, aortic valve calcification is highly correlated with aging. Therefore, the physiological changes in leaflets due to aging (Sahasakul et al., 1988) are an important factor in the biomechanics of CAVD. Specifically, leaflets become thicker and stiffer as a result of aging (Van Geemen et al., 2016). The aortic valve dynamics during CAVD growth is therefore influenced by both calcification and aging.

Different growth and remodeling (G&R) theories have been proposed that enable modeling of tissue adaptation and reorganization (Taber, 1995; Ambrosi et al., 2011; Kuhl, 2014) as a response to pathological stimuli or normal physiological processes. Growth implies the addition of mass by either increasing volume or density. Remodeling implies changes in material properties of the system, which is typically due to reorganization of tissue constituents and fibers and is manifested as changes in stiffness, anisotropy, and degree of nonlinearity. The theory of kinematic growth (finite growth) (Rodriguez et al., 1994) is a popular approach for continuum modeling of G&R and has been applied to different biological tissues (Menzel and Kuhl, 2012; Eskandari et al., 2015; Liu et al., 2019; Lashkarinia et al., 2021).

While the structural mechanics of heart valves have been extensively studied with finite element models (Labrosse et al., 2010; Sturla et al., 2016; Li and Sun, 2017; Qin et al., 2020), very few studies have considered modeling growth in heart valves (Rego et al., 2016; Oomen et al., 2018). Quasi-steady finite element simulations were used to study the influence of aging on aortic valve stress (Oomen et al., 2016). Strain-based calcification growth models have been developed

* Corresponding author.
E-mail address: amir.arzani@nau.edu (A. Arzani).

https://doi.org/10.1016/j.jbiomech.2021.110773
Accepted 22 September 2021
Available online 30 September 2021

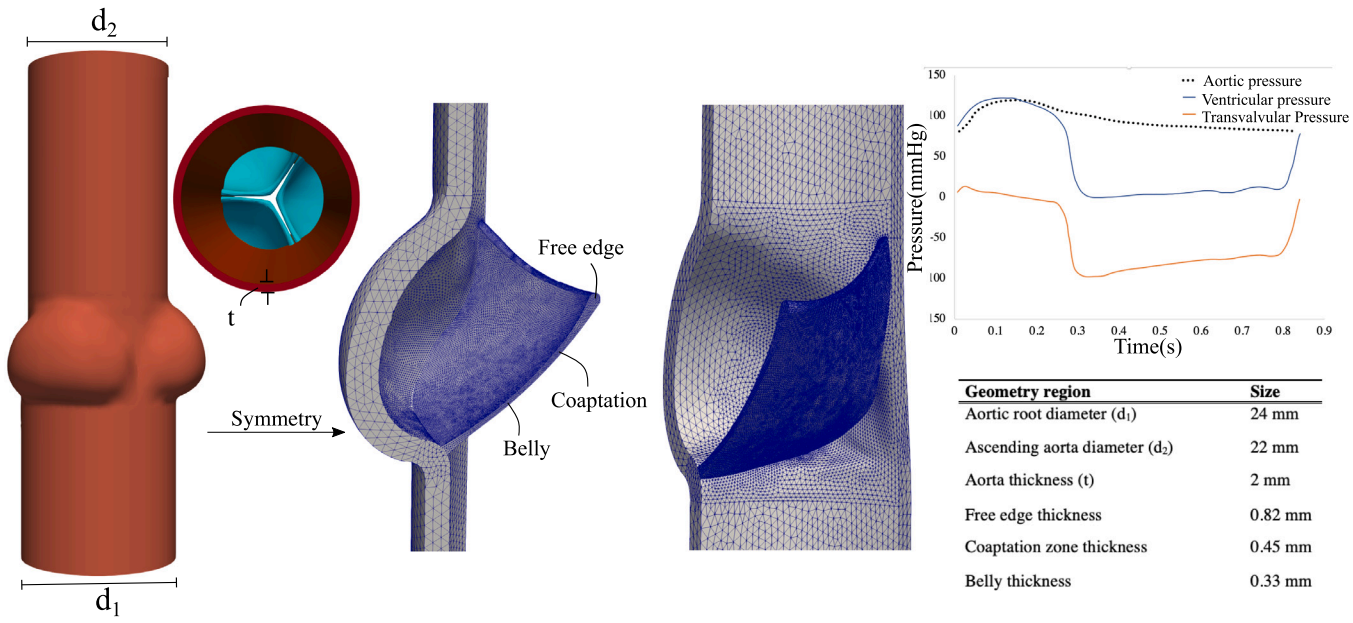

Geometry region	Size
Aortic root diameter (d_1)	24 mm
Ascending aorta diameter (d_2)	22 mm
Aorta thickness (t)	2 mm
Free edge thickness	0.82 mm
Coaptation zone thickness	0.45 mm
Belly thickness	0.33 mm

Fig. 1. Different views of the aortic valve geometry and one-sixth of the geometry (and the corresponding mesh), which is used in the simulations are shown. The prescribed pressure waveform boundary conditions are plotted and the geometric parameters are listed.

where calcification was modeled by local stiffening (Arzani and Mofrad, 2017; Halevi et al., 2018). None of these studies considered a G&R framework in their continuum mechanics formulation. Oomen et al. (2018) developed a quasi-steady G&R model to study the biomechanics of postnatal heart valve development. However, the transient dynamics of the valve, coupling dynamics to G&R, and local G&R due to CAVD have not been studied.

Aortic valve dynamics during CAVD growth is influenced by several processes. Aortic valve calcification is a local process (Thubrikar et al., 1986) where calcification growth is manifested by local stiffening and growth in the aortic valve tissue. CAVD growth is closely related to aging where the valve tissue is known to experience global thickening and stiffening as a result of normal aging (Van Geemen et al., 2016). The process of CAVD growth is therefore a combined physiological and pathological remodeling. In pathological remodeling, typically the remodeling process persists even after the initiating triggers are removed (Schwartz et al., 2018) and therefore a persistence growth process is observed. Calcification growth in CAVD is believed to be such a process where calcium deposition is initiated by inflammatory biochemicals such as lipoproteins and monocytes but persists through a positive feedback loop even without the triggering biochemical stimuli (Pawade et al., 2015).

The goal of the present study is to develop a continuum G&R framework where different biomechanical components during CAVD are modeled. Specifically, we model local growth and remodeling (stiffening) due to calcification combined with global growth and remodeling due to aging. Our formulation considers the transient dynamics of the valve where a temporally multiscale framework is developed to couple G&R occurring over the time-scale of years to transient dynamics with a time scale of one second for valve motion. We use the model to study changes in aortic valve dynamics during CAVD growth and compare our predictions to the data reported in the literature.

2. Methods

2.1. Geometry

An idealized 3D tricuspid aortic valve was assumed as the geometry. The model included the valve leaflet, the aortic root, the sinus, and the ascending aorta (Fig. 1). To simplify the model, the three leaflets were considered to have the same dimensions, and symmetry allowed half of one leaflet to be modeled in order to reduce the computational costs. Aortic root and ascending aorta diameters, and aorta thickness were obtained from previous studies (Joda et al., 2016). The baseline valve dimensions were collected for a healthy 35 years old subject (Weinberg et al., 2009), and the dimensions are reported in Fig. 1. The model was discretized into 360k tetrahedral elements with higher resolution in the leaflet using SimVascular.

2.2. Continuum mechanics model

2.2.1. Deformation gradient

The motion of a body could be defined through a deformation function $\boldsymbol{\phi}$. Particles located at $\mathbf{X}$ in the material or reference configuration β_0 are mapped to $\mathbf{x}$ in the spatial deformed configuration β_t, via $\mathbf{x} = \boldsymbol{\phi}(\mathbf{X}, t)$, where $\boldsymbol{\phi}$ is a function of the initial location and the current time t. Subsequently, the total deformation gradient $\mathbf{F}$ is defined as

$$\mathbf{F} = \nabla \boldsymbol{\phi} \,, \tag{1}$$

where the gradient is with respect to $\mathbf{X}$. The total deformation gradient could be multiplicatively decomposed into elastic and growth components

$$\mathbf{F} = \mathbf{F}_e \mathbf{F}_g \,, \tag{2}$$

where $\mathbf{F}_e$ and $\mathbf{F}_g$ are the elastic and the growth parts of deformation gradient, respectively. $\mathbf{F}_g$ is also known as the growth tensor, and it allows for changes in volume even with incompressible materials (Taber, 2020; Menzel and Kuhl, 2012). In our study, because of different contributions coming from aging and calcification, $\mathbf{F}_g$ has two parts:

$$\mathbf{F}_g = \mathbf{F}_g^{global} + \mathbf{F}_g^{local} \,, \tag{3}$$

where $\mathbf{F}_g^{global}$ represents the global growth of the entire aortic valve due to aging (occurring uniformly in all elements) and $\mathbf{F}_g^{local}$ is the local growth due to calcification (occurring locally in calcified elements). Also, each term on the right-hand side of Eq. (3) could be defined as (Eskandari and Kuhl, 2015):

$$\mathbf{F}_g = \mathbf{I} + \Gamma \mathbf{n} \otimes \mathbf{n} \,, \tag{4}$$

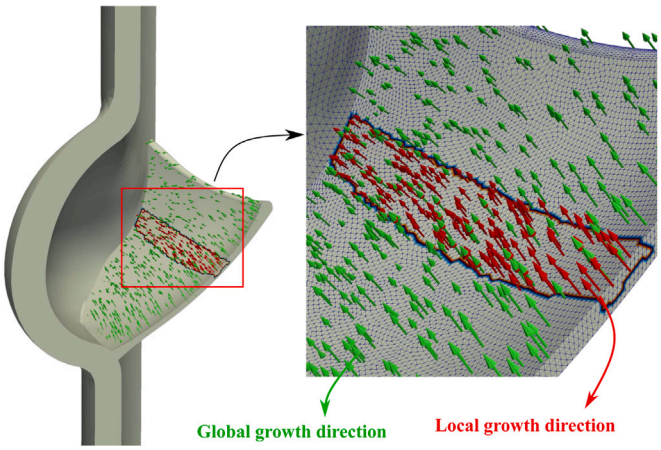

Fig. 2. The global (aging) and local (calcification) growth directions and distribution are shown with green and red arrows, respectively. Local growth is assumed to occur in the coaptation region where calcification often occurs. (For interpretation of the references to color in this figure legend, the reader is referred to the web version of this article.)

where **I** is second order identity tensor, Γ is the growth rate, and **n** is the direction of growth. The direction and location of global and local growth are shown in Fig. 2. Growth direction was assumed normal to the leaflet surface. The local growth is assumed in the coaptation region, which is one of the regions where calcification commonly occurs (Halevi et al., 2015, 2018).

Furthermore, the right Cauchy–Green strain tensor is defined as:

$$\mathbf{C} = \mathbf{F}^T\mathbf{F} = \mathbf{F}_g^T\mathbf{F}_e^T\mathbf{F}_e\mathbf{F}_g = \mathbf{F}_g^T\mathbf{C}_e\mathbf{F}_g. , \tag{5}$$

where the elastic Cauchy–Green tensor is

$$\mathbf{C}_e = \mathbf{F}_e^T\mathbf{F}_e . \tag{6}$$

2.2.2. Cauchy's equation of motion

In the Lagrangian framework, Cauchy's equation of motion is written as (Goriely, 2017):

$$\rho_0\frac{\partial^2\mathbf{U}}{\partial t^2} - \mathrm{Div}(\mathbf{FS}) = \rho_0\mathbf{b}_0 , \tag{7}$$

where $\boldsymbol{\rho_0}$ is the density, **U** is displacement as a function of **X**, **F** is the deformation gradient, $\mathbf{b_0}$ is the body force, Div is divergence with respect to the reference configuration, and **S** is the second Piola–Kirchhoff stress tensor determined from the stain energy function $\boldsymbol{\psi}$ as $\mathbf{S} = 2\frac{\partial\boldsymbol{\psi}}{\partial\mathbf{C}_e}$. Assuming stress-free growth, the deformation due to growth could be considered in the equation of motion by using the elastic part of the deformation gradient ($\mathbf{F}_e = \mathbf{F}\mathbf{F}_g^{-1}$) (Rodriguez et al., 1994).

2.2.3. Material properties

The leaflet was modeled as an anisotropic, nonlinear, nearly incompressible, hyperelastic material (Arzani and Mofrad, 2017; Humphrey and Yin, 1987), and the aortic wall was modeled with a single term Mooney–Rivlin constitutive model (Arzani and Mofrad, 2017; Weinberg and Mofrad, 2007) using the following equations

$$\psi_{valve} = c[e^{(c_1(I_1-3))} - 1] + c_0 f(I_4) \tag{8}$$

$$f(I_4) = \begin{cases} e^{c_2(\sqrt{I_4}-1)^2} - 1 & \text{if } I_4 > 1 \\ 0 & \text{if } I_4 < 1 \end{cases} ,$$

$$\psi_{wall} = c_{wall}(I_1 - 3) , \tag{9}$$

where I_1 is the first invariant of $\mathbf{C}_e$, $I_4 = \mathbf{C}_e : \mathbf{a}_0\otimes\mathbf{a}_0$ is the square of the fiber stretch along the circumferential direction ($\mathbf{a}_0$), c = 0.022 MPa, c_0 = 0.062 MPa, c_{wall} = 0.33 MPa, c_1 = 5.81, and c_2 = 24.97 (Auricchio et al., 2012; Arzani and Mofrad, 2017). The anisotropic term (second term) in Eq. (8) is only switched on when we have stretch in the circumferential direction ($I_4 > 1$).

2.2.4. Finite element implementation

All of the equations are implemented in the open-source finite-element solver FEniCS. The weak form of Cauchy's equation of motion (Eq. (7)) was considered in the reference configuration and solved using quadratic elements. Time integration was performed using the generalized-α method (Chung and Hulbert, 1993).

2.3. Growth algorithm

An algorithm was developed to couple the transient dynamics of the aortic valve in a cardiac cycle with the local/global growth and stiffening effects due to calcification/aging. By applying growth in our algorithm, we impose thickening of the valve leaflet. The vessel wall and leaflet constituents remodeling are represented by simply stiffening the material. Our proposed algorithm has six components and simulates calcification growth and aging for a person between 35 to 85 years old (50 years time interval). In total, we simulated 10 cardiac cycles that were sampled within 824 total growth stages spanning between these ages. 324 cycles for global growth and stiffening and 500 cycles for local growth and stiffening were simulated. More growth stages were considered for the local growth to facilitate numerical convergence

2.3.1. Global growth of the aortic valve due to aging

We assumed that due to aging the thickness of the valve leaflet increases uniformly over time. Global growth of the aortic valve was assumed quasi-static, therefore the acceleration term in Eq. (7) was eliminated when each growth stage was applied. The direction of the growth was assumed to be normal to the surface of the leaflet (Fig. 2). The total leaflet thickness growth over these 50 years (35 to 85 years old) was assumed to be 81% of the baseline configuration (estimated from Sahasakul et al. (1988)). Due to numerical difficulties associated with the Newton solver convergence and the complex geometry, 324 cycles of global growth were simulated in which a small steady 0.25% growth rate (with respect to the healthy reference configuration) was added in each global growth cycle to achieve the desired 81% growth.

2.3.2. Global stiffening of the aortic valve due to aging

Aortic valve stiffening due to aging was estimated based on the reported module of elasticities in previous studies (Van Geemen et al., 2016). The c and c_0 constants in Eq. (8) were increased linearly during 50 years such that the final stiffness was 2.32 times the baseline. The stiffenings were applied during the same stages as global growth.

2.3.3. Global stiffening of the aortic wall due to aging

The aortic wall stiffness, c_{wall} in Eq. (9), was increased linearly such that after 50 years its value was 2.68 times larger than the baseline based on clinical data of Haskett et al. (2010). The stiffenings were applied during the same stages as global growth.

2.3.4. Local growth of the aortic valve due to calcification

The calcification pattern was assumed to be around the coaptation area based on prior clinical studies (Halevi et al., 2018; Thubrikar et al., 1986). This region is one of the two most common calcification patterns observed (Thubrikar et al., 1986). We assumed that the calcification process starts at 60 years old (representing calcification at an older age). The first two layers of elements in the aortic side of the leaflet were tagged for calcification, based on the clinical observation that calcification is more likely to occur on the aortic side (Otto et al., 1994; Yip and Simmons, 2011). 100% local growth for these two layers was prescribed from 60 to 85 years old. In other words, the F_g^{local} term in Eq. (3) was switched on after year 60. In total, 500 local growth stages were simulated and in each stage, the growth rate (with respect to the healthy reference configuration) was increased linearly by 0.2% to achieve the 100% local growth.

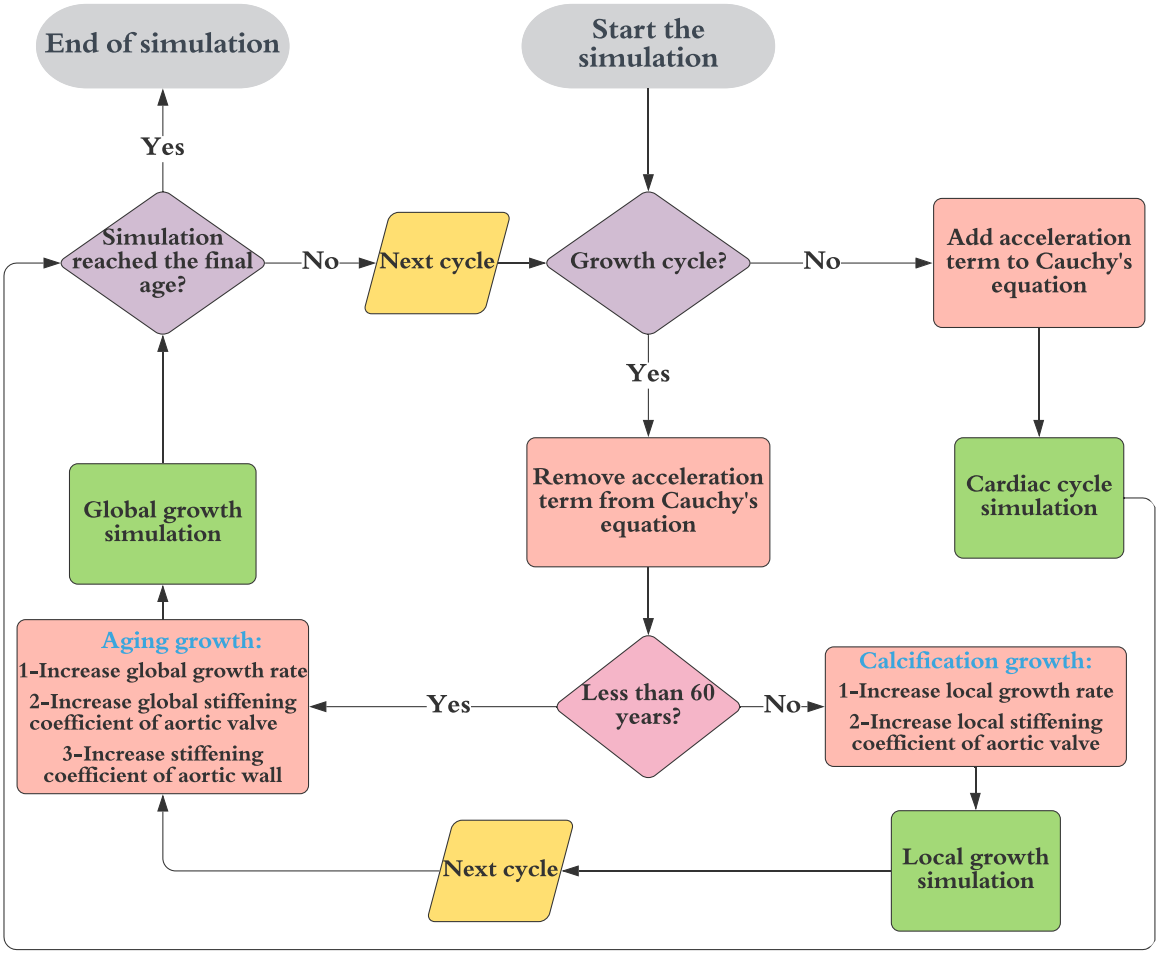

Fig. 3. The algorithm used in simulating long-term calcification and aging coupled with transient dynamics of the valve.

2.3.5. Local stiffening of the aortic valve due to calcification

Calcification causes valve thickening and stiffening. Stiffening was modeled for the same elements that were tagged for local growth due to calcification. In this part, it was assumed that calcification increases the isotropic material constant **c** (Arzani and Mofrad, 2017). The constant was increased linearly such that at the end of 85 years old, it was 100 times more than the baseline value, representing the stiffening caused by calcium deposits (Wong et al., 2012; Holzapfel et al., 2002). Local stiffening was applied during each local growth stage.

2.3.6. Dynamics of the valve

Global and local growth and stiffening were considered to happen over the timescale of years. However, each heartbeat is about one second. In Cauchy's equation of motion (Eq. (7)), the first left-hand-side term (acceleration term) was assumed zero when each growth step was first being prescribed. However, during the corresponding transient cardiac cycle simulation, the acceleration term was considered. Boundary conditions (BCs) include fixing the vessel wall in the circumferential and axial directions at the ends (zero Dirichlet BC) and pulsatile pressure waveforms (shown in Fig. 1) applied at the vessel wall and leaflet (Neumann BC) driving the transient tissue dynamics. The flowchart of the algorithm summarizing all of the stages is sketched in Fig. 3.

2.4. Strain-based local growth and remodeling

To study heterogeneous growth, which occurs due to the complex hemodynamic environment, we modeled local growth and remodeling driven by strain. During each growth stage, the updated time-average circumferential strain in one cardiac cycle was calculated, and the elements with strain higher than a pre-specified threshold of 0.07 were calcified (Fisher et al., 2013; Arzani and Mofrad, 2017). This was done by 100% local thickening of the elements and stiffening by a factor of 100. To enable numerical convergence, the 100% local thickening was achieved with 500 sub-growth steps. This algorithm was repeated until the strain field was below the specified threshold. Global G&R (aging) was not considered during these simulations to reduce the computational cost.

3. Results

3.1. Model validation

First, the dynamics of the healthy valve at the start of our aging simulation (35 years old) was compared to previous studies (Jahren et al., 2017; Spühler et al., 2018; Lee et al., 2020). The intra-cardiac evolution of the geometric orifice area (GOA) is calculated as explained in Garcia and Kadem (2006) and is shown in Fig. 4a. Additionally, the temporal evolution of displacement for a point at the leaflet's free edge and belly for the healthy case were compared with other studies (Thubrikar, 1990; Weinberg and Mofrad, 2007) as shown Fig. 4b and Fig. 4c respectively. Reasonable agreement between our idealized model and other studies is observed for all of these results.

3.2. Growth results

GOA results for different ages (35 years old to 85 years old) are reported in Fig. 5. The results show a lower reduction in GOA during the

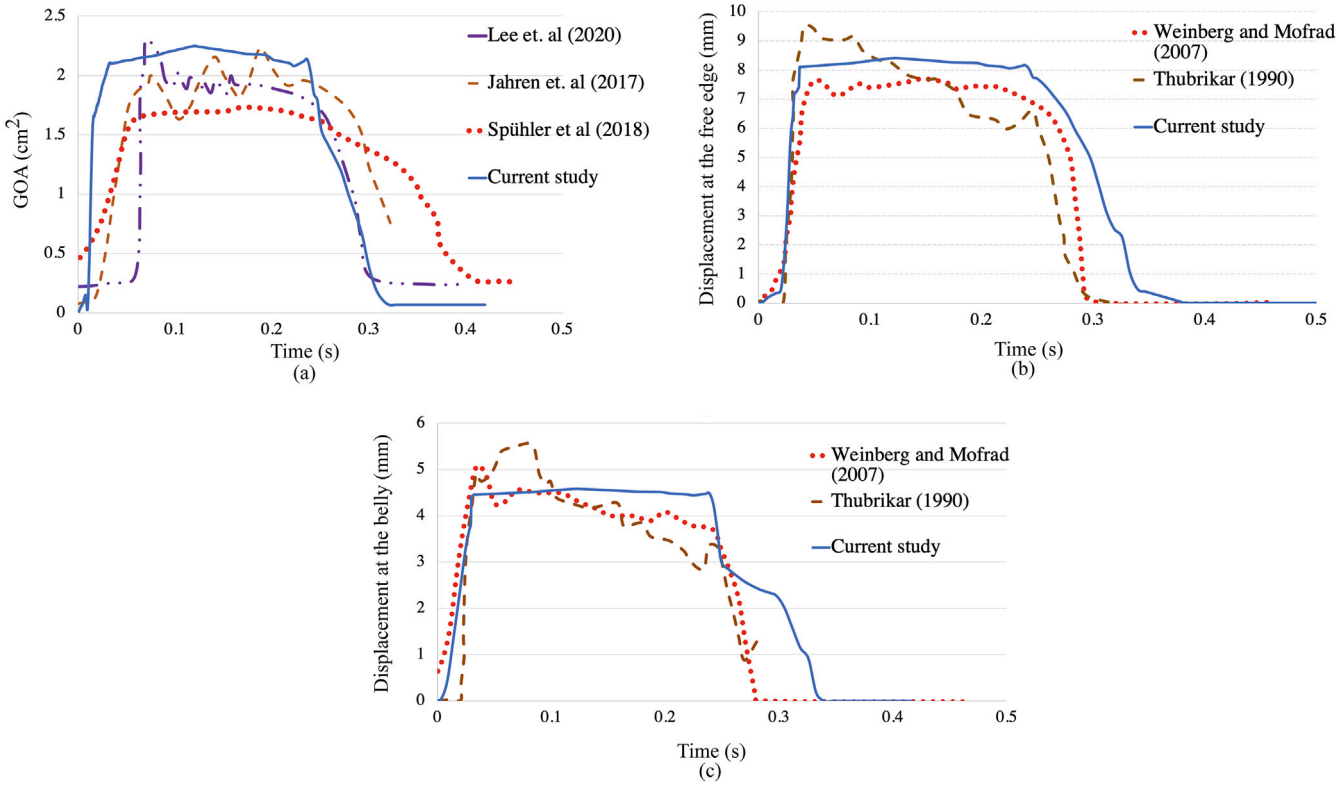

Fig. 4. The dynamics of the valve at the baseline healthy age is compared with other studies. (a) The geometric orifice area (GOA), (b) displacement of a point at the free edge, (c) and displacement of a point at the belly (middle of the valve) are compared to other studies.

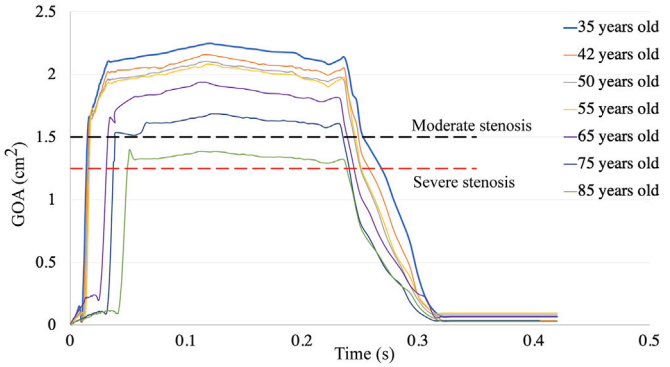

Fig. 5. The intra-cardiac temporal evolution of the geometric orifice area (GOA) during different ages is plotted. GOA for severe stenosis (1.3 cm^2) is reported in Clavel et al. (2015) and Westermann et al. (2011), and the GOA for moderate stenosis (1.5 cm^2) is reported in Baumgartner et al. (2017).

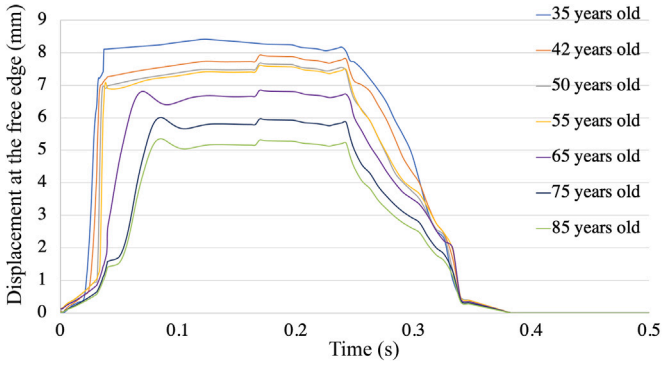

Fig. 6. The intra-cardiac temporal evolution of displacement for a point at the middle of the free edge (symmetry plane) during different ages is plotted.

early years when only the global growth and stiffening were applied to the model. However, after year 60 when calcification (local growth and stiffening) is applied, the GOA reduction is elevated. The GOA of the 75 years old model was near the moderate stenosis level (Baumgartner et al., 2017), and the GOA of the 85 years old was near the severe stenosis level that was reported in clinical studies (Westermann et al., 2011; Clavel et al., 2015).

The intra-cardiac temporal displacement patterns of a point at the leaflet's free edge for different ages (35 years old to 85 years old) are plotted in Fig. 6. As expected, with increased aging the displacement is reduced. Interestingly, the displacement patterns of the healthy 35 years old subject, cases between 35 years to 60 years old (global growth and stiffening), and the cases after 60 years old (global and local growth and stiffening) are distinct. For example, the rapid valve opening time increases suddenly after age 60 when the calcification was added to the model. Similar to the GOA results, the largest reduction in displacement occurs after calcification was applied (after 60 years old).

The spatial patterns of displacement during peak systole and leaflet tissue growth during diastole are shown in Fig. 7 for four different ages. The global thickening of the aortic valve leaflet due to aging and local thickening due to calcification (after 60 years old) could be observed. Additionally, the effect of leaflet thickening and stiffening during different ages on valve opening patterns is observed.

The Von-Mises stress and circumferential strain are shown in Fig. 8 for four different ages during diastole (the color bar range is different in different plots). It can be seen that the distribution of stress on the leaflet changes at different ages. The maximum stress value is increased during aging. The maximum stress occurs at the leaflet attachment during most ages. However, with significant growth of calcification at

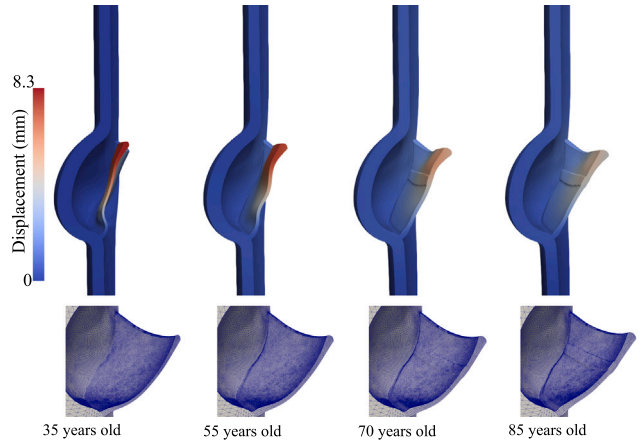

Fig. 7. Spatial patterns of valve opening and displacement (top row) and the local/global thickening of the valve leaflet during diastole (bottom row) are shown for four different ages. Local growth/stiffening due to calcification starts at age 60.

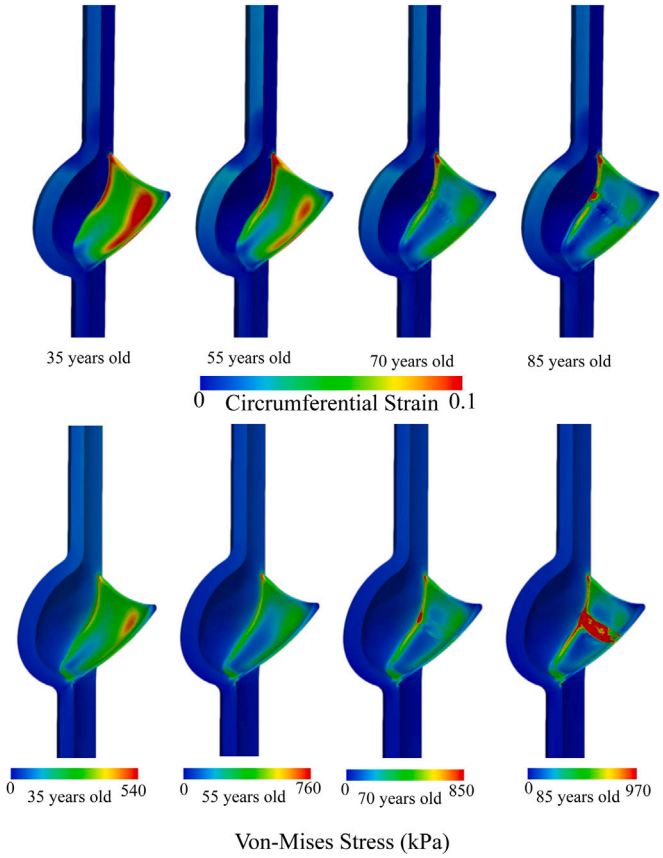

Fig. 8. Circumferential strain and the Von-Mises stress are shown during diastole for four different ages. Local growth/stiffening due to calcification starts at age 60. (For interpretation of the references to color in this figure legend, the reader is referred to the web version of this article.)

age 85, a localized increase in stress is observed in the calcification region due to compliance mismatch and growth-associated residual stress. The circumferential strain is generally reduced due to thickening and stiffening.

Rapid valve opening time (RVOT), which is defined as the time it takes for the valve leaflet to become fully opened is compared to the data in the literature. RVOT values are reported in Table 1 for healthy

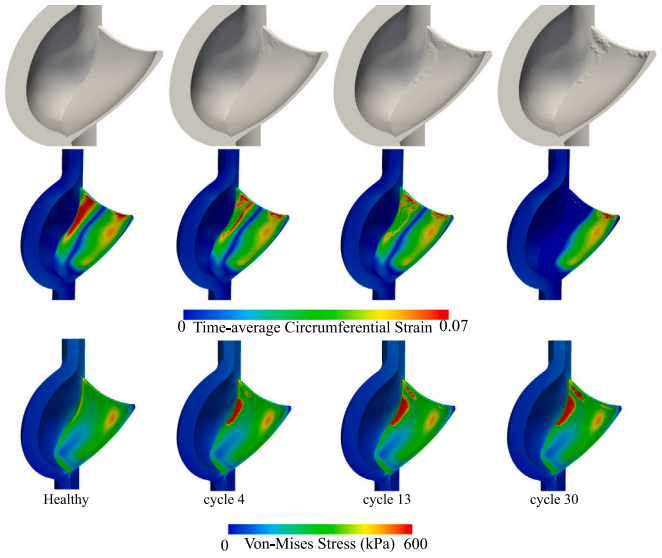

Fig. 9. The local growth patterns due to calcification (top row), the time-average circumferential strain (middle row), and the diastolic Von-Mises stress are shown for four different cycles in the strain-based calcification model (local growth and remodeling). .

Table 1
Comparison between the rapid valve opening time (RVOT) in the current study and the data reported in the literature.

Configuration	RVOT (ms)
Healthy aortic valve	
35 years old (current study)	41
Maleki et al. (2014) (numerical simulation data)	50
Maleki et al. (2014) (experimental data)	60
Tango et al. (2021) (numerical simulation data)	50
Kemp et al. (2013) (numerical simulation data)	40
Kemp et al. (2013) (experimental data)	37 ± 3
Leyh et al. (1999) (experimental data)	57 ± 11
Aortic valve with severe stenosis	
85 years old (current study)	86
Maleki et al. (2014) (numerical simulation data)	100
Maleki et al. (2014) (experimental data)	72

and severely stenosed aortic valves and are compared with the numerical and experimental data in Leyh et al. (1999), Kemp et al. (2013), Maleki et al. (2014) and Tango et al. (2021). The results indicate that RVOT is increased during aging and a fairly good agreement is seen between our results and those reported in the literature.

The results for the strain-based local G&R are shown in Fig. 9. Thirty cycles of growth were simulated, after which no element had strain greater than the pre-specified threshold and therefore the algorithm stopped. The local calcification growth pattern together with the time-average circumferential strain and Von-Mises stress results are shown. In regions where calcification became established, the time-average circumferential strain was reduced due to the stiffening and growth.

4. Discussion

CAVD growth influences aortic valve biomechanics in multiple ways. In this study, we developed a G&R framework to model long-term calcification growth and aging coupled with transient valve dynamics. The model enables automated simulation of intra-cardiac aortic valve dynamics within the process of CAVD growth. The model was used to study changes in the aortic valve opening patterns (tip displacement and GOA) and structural stress during a 50-year time span of aging and calcification growth.

There are two leading theories for the G&R of soft tissues (Ambrosi et al., 2019): 1- The constrained mixture theory, in which each

constituent in the tissue, such as vascular cells and collagen fibers, can change at different rates and control different stress-free configurations that evolve during G&R while deforming as a continuum model (Humphrey and Rajagopal, 2002). 2- Kinematic growth, which is based on the multiplicative decomposition of the deformation gradient into elastic and growth components (Rodriguez et al., 1994). Modeling constrained mixture growth is highly complex because it is hard to track the evolving configuration of the constituents during G&R (Lee et al., 2016). In this manuscript, because of the complex geometry and coupling to nonlinear and highly transient dynamics, the latter theory was preferred.

In the kinematic theory, there is a relationship between stress generated within the tissue and tissue growth. Stress dependent growth and residual stress arising from growth are two different mechanisms of the kinematic growth theory (Rodriguez et al., 1994). The first mechanism has been used to show how soft tissues grow due to overload in stress. For example, high blood pressure in the ventricles causes heart hypertrophy (Genet et al., 2016). In our work, the first mechanism was modeled with our strain-based growth model. Regarding the second mechanism, aging caused by fibrosis and collagen degeneration leads to growth and thickening in the aortic valve (Sell and Scully, 1965). This thickening was modeled by our global growth approach and leads to an increase in the residual stress in the leaflet. For example, by comparing the stress value of 35 and 55 years old cases in Fig. 8, the peak stress is observed to increase with age. The stress increment is higher near the attachment of the leaflet, and it may contribute to calcification, which often starts from the attachment region (Thubrikar et al., 1986). Additionally, the locally elevated stress generated in the calcification region could be a potential risk factor for stroke (Sturla et al., 2016) by detaching the calcium deposits and generating emboli that could travel to the brain.

The propagation phase of CAVD is driven by high mechanical stretch (Pawade et al., 2015; Arzani and Mofrad, 2017). That is, calcification, followed by G&R, is a function of stress and strain. Although there may be a nonlinear relationship between G&R and stress, we simplified the model by increasing the growth rate value linearly and assuming a pre-defined calcification pattern. Also, we applied local growth for a band in the first two layers of elements on the fibrosa side of the leaflet. Interestingly, abnormal deformation of the elements on the ventricular side of the leaflet was observed (results not shown). Since the growth tensor $\mathbf{F}_g$ is incompatible locally, elastic deformation is required to maintain the continuity of the leaflet. Our model highlights two stress-driven mechanisms associated with G&R in CAVD. The local remodeling (stiffening) due to calcification causes stress concentration, which has been previously linked with calcification growth (Pawade et al., 2015; Arzani and Mofrad, 2017). Moreover, local and global growth in thickness generates residual stress. We hypothesize that these mechanisms together promote CAVD growth.

The complex geometry induced by local growth causes numerical difficulties, particularly when coupled with a nonlinear transient solver with large structural deformations. To improve the numerical convergence of the nonlinear Newton solver in FEniCS, we reduced the growth rate in the local and global growth models. This led to several hundred cycles of growth in our simulation. However, the interesting feature of our model is that the transient cardiac cycle simulations do not necessarily need to be carried out at every growth step. We may think of this as a temporally multiscale model. The time-scale for transient dynamics is on the order of one second, whereas the time-scale for G&R is months and years.

Our study has several limitations. While we studied non-uniform local growth based on strain, non-uniform global growth due to aging was not modeled due to lack of sufficient data. Although we defined variable thickness dimensions for our geometry based on previous studies and clinical data, our geometry is still idealized and needs to be extended to patient-specific geometries. Our constitutive model could also be improved. For example, Gasser et al. (2006) and Dong and Sun (2021) represent fiber dispersion for vascular tissues, which was not considered here. These more complex models could influence the intra-cardiac elastodynamics patterns but we expect the overall growth patterns to be similar. Fluid–structure interaction (FSI) and hemodynamics were ignored but are known to influence aortic valve dynamics (Luraghi et al., 2017). Other growth mechanisms exist during CAVD; for example, glycosaminoglycans are known to play a role in CAVD (Porras et al., 2018), which could influence valve biomechanics by swelling and could be considered in G&R models (Roccabianca et al., 2014). The biochemical stimuli in the G&R associated with CAVD were not considered and require FSI transport models (Sadrabadi et al., 2021) to be appropriately incorporated. These limitations will be addressed by a growing interest in coupling systems biology models with continuum models of disease growth to develop multiscale mechanobiology models (Loerakker and Ristori, 2020; Sree and Tepole, 2020). Future work will consider mechano-sensitive microscale biochemical effects coupled with macroscale continuum G&R to develop a comprehensive model of CAVD growth. In general, growth is a manifestation of biological processes and affects the biomechanical environment. Additionally, the biomechanical environment regulates biological activities, thereby creating a feedback loop that has been referred to as the "hallmark of mechanobiology" (Taber, 2020).

5. Conclusion

We developed a G&R framework for simulating long-term calcification growth and aging during CAVD growth. Our model incorporated transient dynamics of the aortic valve within the G&R framework and was used to study changes in aortic valve dynamics and stress during CAVD growth and aging. This model could be coupled with cell-scale models of CAVD to develop a multiscale systems mechanobiology model of CAVD.

Declaration of competing interest

The authors declare that they have no known competing financial interests or personal relationships that could have appeared to influence the work reported in this paper.

Acknowledgment

This study was supported by funding from NSF, United States OAC grant No. 1947559.

References

Ambrosi, D., Ateshian, G.A., Arruda, E.M., Cowin, S.C., Dumais, J., Goriely, A., Holzapfel, G.A., Humphrey, J.D., Kemkemer, R., Kuhl, E., et al., 2011. Perspectives on biological growth and remodeling. J. Mech. Phys. Solids 59 (4), 863–883.

Ambrosi, D., Ben Amar, M., Cyron, C.J., DeSimone, A., Goriely, A., Humphrey, J.D., Kuhl, E., 2019. Growth and remodelling of living tissues: perspectives, challenges and opportunities. J. Royal Soc. Interface 16 (157), 20190233.

Arzani, A., Masters, K.S., Mofrad, M.R.K., 2017. Multiscale systems biology model of calcific aortic valve disease progression. ACS Biomater. Sci. & Eng. 3 (11), 2922–2933.

Arzani, A., Mofrad, M.R.K., 2017. A strain-based finite element model for calcification progression in aortic valves. J. Biomech. 65, 216–220.

Auricchio, F., Ferrara, A., Morganti, S., 2012. Comparison and critical analysis of invariant-based models with respect to their ability in fitting human aortic valve data. Ann. Solid Struct. Mech. 4 (1–2), 1–14.

Baumgartner, H., Hung, J., Bermejo, J., Chambers, J.B., Edvardsen, T., Goldstein, S., Lancellotti, P., LeFevre, M., Miller Jr, F., Otto, C.M., et al., 2017. Recommendations on the echocardiographic assessment of aortic valve stenosis: a focused update from the european association of cardiovascular imaging and the american society of echocardiography. Eur. Heart J.-Cardiovasc. Imaging 18 (3), 254–275.

Carabello, B.A., Paulus, W.J., 2009. Aortic stenosis. Lancet 373 (9667), 956–966.

Chung, J., Hulbert, G.M., 1993. A time integration algorithm for structural dynamics with improved numerical dissipation: The generalized-α method. J. Appl. Mech. 60 (2), 371–375.

Clavel, M., Malouf, J., Messika-Zeitoun, D., Araoz, P.A., Michelena, H.I., Enriquez-Sarano, M., 2015. Aortic valve area calculation in aortic stenosis by ct and doppler echocardiography. JACC: Cardiovasc. Imaging 8 (3), 248–257.

Dong, H., Sun, W., 2021. A novel hyperelastic model for biological tissues with planar distributed fibers and a second kind of Poisson effect. J. Mech. Phys. Solids 151, 104377.

Eskandari, M., Kuhl, E., 2015. Systems biology and mechanics of growth. Wiley Interdiscip. Rev.: Syst. Biol. Med. 7 (6), 401–412.

Eskandari, M., Kuschner, W.G., Kuhl, E., 2015. Patient-specific airway wall remodeling in chronic lung disease. Ann. Biomed. Eng. 43 (10), 2538–2551.

Fisher, C.I., Chen, J., Merryman, W.D., 2013. Calcific nodule morphogenesis by heart valve interstitial cells is strain dependent. Biomech. Model. Mechanobiol. 12 (1), 5–17.

Garcia, D., Kadem, L., 2006. What do you mean by aortic valve area: geometric orifice area, effective orifice area, or gorlin area? J. Heart Valve Dis. 15 (5), 601.

Gasser, T.C., Ogden, R.W., Holzapfel, G.A., 2006. Hyperelastic modelling of arterial layers with distributed collagen fibre orientations. J. R. Soc. Interface 3 (6), 15–35.

Genet, M., Lee, L.C., Baillargeon, B., Guccione, J.M., Kuhl, E., 2016. Modeling pathologies of diastolic and systolic heart failure. Ann. Biomed. Eng. 44 (1), 112–127.

Goriely, A., 2017. The Mathematics and Mechanics of Biological Growth. p. 45.

Halevi, R., Hamdan, A., Marom, G., Lavon, K., Ben-Zekry, S., Raanani, E., Haj-Ali, R., 2018. A new growth model for aortic valve calcification. J. Biomech. Eng. 140 (10).

Halevi, R., Hamdan, A., Marom, G., Mega, M., Raanani, E., Haj-Ali, R., 2015. Progressive aortic valve calcification: three-dimensional visualization and biomechanical analysis. J. Biomech. 48 (3), 489–497.

Haskett, D., Johnson, G., Zhou, A., Utzinger, U., Geest, J.V., 2010. Microstructural and biomechanical alterations of the human aorta as a function of age and location. Biomech. Model. Mechanobiol. 9 (6), 725–736.

Hatoum, H., Dasi, L.P., 2019. Spatiotemporal complexity of the aortic sinus vortex as a function of leaflet calcification. Ann. Biomed. Eng. 47 (4), 1116–1128.

Hatoum, H., Dollery, J., Lilly, S.M., Crestanello, J.A., Dasi, L.P., 2018. Effect of severe bioprosthetic valve tissue ingrowth and inflow calcification on valve-in-valve performance. J. Biomech. 74, 171–179.

Holzapfel, G.A., Stadler, M., Schulze-Bauer, C.A.J., 2002. A layer-specific three-dimensional model for the simulation of balloon angioplasty using magnetic resonance imaging and mechanical testing. Ann. Biomed. Eng. 30 (6), 753–767.

Humphrey, J.D., Rajagopal, K.R., 2002. A constrained mixture model for growth and remodeling of soft tissues. Math. Models Methods Appl. Sci. 12 (03), 407–430.

Humphrey, J.D., Yin, F.C.P., 1987. On constitutive relations and finite deformations of passive cardiac tissue: I. a pseudostrain–energy function. J. Biomech. Eng. 109 (4), 298–304.

Jahren, S.E., Winkler, B.M., Heinisch, P.P., Wirz, J., Carrel, T., Obrist, D., 2017. Aortic root stiffness affects the kinematics of bioprosthetic aortic valves. Interact. Cardiovasc. Thorac. Surg. 24 (2), 173–180.

Joda, A., Jin, Z., Haverich, A., Summers, J., Korossis, S., 2016. Multiphysics simulation of the effect of leaflet thickness inhomogeneity and material anisotropy on the stress–strain distribution on the aortic valve. J. Biomech. 49 (12), 2502–2512.

Kemp, I., Dellimore, K., Rodriguez, R., Scheffer, C., Blaine, D., Weich, H., Doubell, A., 2013. Experimental validation of the fluid–structure interaction simulation of a bioprosthetic aortic heart valve. Australas. Phys. Eng. Sci. Med. 36 (3), 363–373.

Kuhl, E., 2014. Growing matter: a review of growth in living systems. J. Mech. Behav. Biomed. Mater. 29, 529–543.

Labrosse, M.R., Lobo, K., Beller, C.J., 2010. Structural analysis of the natural aortic valve in dynamics: from unpressurized to physiologically loaded. J. Biomech. 43 (10), 1916–1922.

Lashkarinia, S.S., Coban, G., Kose, B., Salihoglu, E., Pekkan, K., 2021. Computational modeling of vascular growth in patient-specific pulmonary arterial patch reconstructions. J. Biomech. 117, 110274.

Lee, L.C., Kassab, G.S., Guccione, J.M., 2016. Mathematical modeling of cardiac growth and remodeling. Wiley Interdiscip. Rev.: Syst. Biol. Med. 8 (3), 211–226.

Lee, J.H., Rygg, A.D., Kolahdouz, E.M., Rossi, S., Retta, S.M., Duraiswamy, N., Scotten, L.N., Craven, B.A., Griffith, B.E., 2020. Fluid–structure interaction models of bioprosthetic heart valve dynamics in an experimental pulse duplicator. Ann. Biomed. Eng. 1–16.

Leyh, R.G., Schmidtke, C., Sievers, H.H., Yacoub, M.H., 1999. Opening and closing characteristics of the aortic valve after different types of valve-preserving surgery. Circulation 100 (21), 2153–2160.

Li, K., Sun, W., 2017. Simulated transcatheter aortic valve deformation: A parametric study on the impact of leaflet geometry on valve peak stress. Int. J. Numer. Methods Biomed. Eng. 33 (3), e02814.

Liu, H., Zhang, M., Liu, M., Martin, C., Cai, Z., Sun, W., 2019. Finite element simulation of three dimensional residual stress in the aortic wall using an anisotropic tissue growth model. J. Mech. Behav. Biomed. Mater. 92, 188–196.

Loerakker, S., Ristori, T., 2020. Computational modeling for cardiovascular tissue engineering: the importance of including cell behavior in growth and remodeling algorithms. Curr. Opin. Biomed. Eng. 15, 1–9.

Luraghi, G., Wu, W., De Gaetano, F., Matas, J.F.R., Moggridge, G.D., Serrani, M., Stasiak, J., Costantino, M.L., Migliavacca, F., 2017. Evaluation of an aortic valve prosthesis: Fluid–structure interaction or structural simulation? J. Biomech. 58, 45–51.

Maleki, H., Shahriari, S., Durand, L.G., Labrosse, M.R., Kadem, L., 2014. A metric for the stiffness of calcified aortic valves using a combined computational and experimental approach. Med. Biol. Eng. Comput. 52 (1), 1–8.

Menzel, A., Kuhl, E., 2012. Frontiers in growth and remodeling. Mech. Res. Commun. 42, 1–14.

Oomen, P.J.A., Holland, M.A., Bouten, C.V.C., Kuhl, E., Loerakker, S., 2018. Growth and remodeling play opposing roles during postnatal human heart valve development. Sci. Rep. 8 (1), 1–13.

Oomen, P.J.A., Loerakker, S., Van Geemen, D., Neggers, J., Goumans, M.J.T.H, Van Den Bogaerdt, A.J., Bogers, A.J.J.C, Bouten, C.V.C., Baaijens, F.P.T., 2016. Age-dependent changes of stress and strain in the human heart valve and their relation with collagen remodeling. Acta Biomater. 29, 161–169.

Otto, C.M., Burwash, I.G., Legget, M.E., Munt, B.I., Fujioka, M., Healy, N.L., Kraft, C.D., Miyake-Hull, C.Y., Schwaegler, R.G., 1997. Prospective study of asymptomatic valvular aortic stenosis: clinical, echocardiographic, and exercise predictors of outcome. Circulation 95 (9), 2262–2270.

Otto, C.M., Kuusisto, J., Reichenbach, D.D., Gown, A.M., O'Brien, K.D., 1994. Characterization of the early lesion of'degenerative'valvular aortic stenosis. histological and immunohistochemical studies. Circulation 90 (2), 844–853.

Pawade, T.A., Newby, D.E., Dweck, M.R., 2015. Calcification in aortic stenosis: the skeleton key. J. Am. Coll. Cardiol. 66 (5), 561–577.

Porras, A.M., Westlund, J.A., Evans, A.D., Masters, K.S., 2018. Creation of disease-inspired biomaterial environments to mimic pathological events in early calcific aortic valve disease. Proc. Natl. Acad. Sci. 115 (3), 363–371.

Qin, T., Caballero, A., Mao, W., Barrett, B., Kamioka, N., Lerakis, S., Sun, W., 2020. The role of stress concentration in calcified bicuspid aortic valve. J. R. Soc. Interface 17 (167), 20190893.

Rego, B.V., Wells, S.M., Lee, C.H., Sacks, M.S., 2016. Mitral valve leaflet remodelling during pregnancy: insights into cell-mediated recovery of tissue homeostasis. J. R. Soc. Interface 13 (125), 20160709.

Roccabianca, S., Bellini, C., Humphrey, J.D., 2014. Computational modelling suggests good, bad and ugly roles of glycosaminoglycans in arterial wall mechanics and mechanobiology. J. R. Soc. Interface 11 (97), 20140397.

Rodriguez, E.K., Hoger, A., McCulloch, A.D., 1994. Stress-dependent finite growth in soft elastic tissues. J. Biomech. 27 (4), 455–467.

Sadrabadi, M.S., Hedayat, M., Borazjani, I., Arzani, A., 2021. Fluid–structure coupled biotransport processes in aortic valve disease. J. Biomech. 117, 110239.

Sahasakul, Y., Edwards, W.D., Naessens, J.M., Tajik, A.J., 1988. Age-related changes in aortic and mitral valve thickness: implications for two-dimensional echocardiography based on an autopsy study of 200 normal human hearts. Am. J. Cardiol. 62 (7), 424–430.

Schwartz, M.A., Vestweber, D., Simons, M., 2018. A unifying concept in vascular health and disease. Science 360 (6386), 270–271.

Sell, S., Scully, R.E., 1965. Aging changes in the aortic and mitral valves: histologic and histochemical studies, with observations on the pathogenesis of calcific aortic stenosis and calcification of the mitral annulus. Am. J. Pathol. 46 (3), 345.

Spühler, J.H., Jansson, J., Jansson, N., Hoffman, J., 2018. 3d fluid–structure interaction simulation of aortic valves using a unified continuum ale fem model. Front. Physiol. 9, 363.

Sree, V.D., Tepole, A.B., 2020. Computational systems mechanobiology of growth and remodeling: Integration of tissue mechanics and cell regulatory network dynamics. Curr. Opin. Biomed. Eng. 15, 75–80.

Sturla, F., Ronzoni, M., Vitali, M., Dimasi, A., Vismara, R., Preston-Maher, G., Burriesci, G., Votta, E., Redaelli, A., 2016. Impact of different aortic valve calcification patterns on the outcome of transcatheter aortic valve implantation: a finite element study. J. Biomech. 49 (12), 2520–2530.

Taber, L.A., 1995. Biomechanics of growth, remodeling, and morphogenesis. Appl. Mech. Rev. 48 (8), 487–545.

Taber, L.A., 2020. Continuum Modeling in Mechanobiology. Springer.

Tango, A.M., Ducci, A., Burriesci, G., 2021. In silico study of the ageing effect upon aortic valves. J. Fluids Struct. 103, 103258.

Thaden, J.J., Nkomo, V.T., Enriquez-Sarano, M., 2014. The global burden of aortic stenosis. Prog. Cardiovasc. Dis. 56 (6), 565–571.

Thubrikar, M.J., 1990. The Aortic Valve. CRC Press.

Thubrikar, M.J., Aouad, J., Nolan, S.P., 1986. Patterns of calcific deposits in operatively excised stenotic or purely regurgitant aortic valves and their relation to mechanical stress. Am. J. Cardiol. 58 (3), 304–308.

Van Geemen, D., Soares, A.L.F., Oomen, P.J.A., Driessen-Mol, A., Janssen-van den Broek, M.W.T., Van Den Bogaerdt, A.J., Bogers, A.J.J.C, Goumans, M.T., Baaijens, F.P., Bouten, C.V., 2016. Age-dependent changes in geometry, tissue composition and mechanical properties of fetal to adult cryopreserved human heart valves. PLoS One 11 (2), e0149020.

Weinberg, E.J., Mofrad, M.R.K., 2007. Transient, three-dimensional, multiscale simulations of the human aortic valve. Cardiovasc. Eng. 7 (4), 140–155.

Weinberg, E.J., Schoen, F.J., Mofrad, M.R.K., 2009. A computational model of aging and calcification in the aortic heart valve. PLoS One 4 (6), e5960.

Weinberg, E.J., Shahmirzadi, D., Mofrad, M.R.K., 2010. On the multiscale modeling of heart valve biomechanics in health and disease. Biomech. Model. Mechanobiol. 9 (4), 373–387.

Westermann, Y., Geigenmüller, A., Elgeti, T., Wagner, M., Dushe, S., Borges, A.C., Dohmen, P.M., Hein, P.A., Lembcke, A., 2011. Planimetry of the aortic valve orifice area: comparison of multislice spiral computed tomography and magnetic resonance imaging. Eur. J. Radiol. 77 (3), 426–435.

Wong, K.K.L., Thavornpattanapong, P., Cheung, S.C.P., Sun, Z., Tu, J., 2012. Effect of calcification on the mechanical stability of plaque based on a three-dimensional carotid bifurcation model. BMC Cardiovasc. Disord. 12 (1), 1–18.

Yip, C.Y.Y., Simmons, C.A., 2011. The aortic valve microenvironment and its role in calcific aortic valve disease. Cardiovasc. Pathol. 20 (3), 177–182.